Estimating decadal variability in sea level from tide gauge records
An application to the North Sea

Frederikse, Thomas; Riva, Riccardo; Slobbe, Cornelis; Broerse, Taco; Verlaan, Martin

DOI
10.1002/2015JC011174

Publication date
2016

Document Version
Final published version

Published in
Journal Of Geophysical Research-Oceans

Citation (APA)
Frederikse, T., Riva, R., Slobbe, C., Broerse, T., & Verlaan, M. (2016). Estimating decadal variability in sea level from tide gauge records: An application to the North Sea. *Journal Of Geophysical Research-Oceans*, *121*(3), 1529-1545. https://doi.org/10.1002/2015JC011174

AGU PUBLICATIONS

JGR

Journal of Geophysical Research: Oceans

RESEARCH ARTICLE

10.1002/2015JC011174

Estimating decadal variability in sea level from tide gauge records: An application to the North Sea

Thomas Frederikse[1], Riccardo Riva[1], Cornelis Slobbe[1], Taco Broerse[1], and Martin Verlaan[2,3]

[1]Department of Civil Engineering and Geosciences, Delft University of Technology, Delft, Netherlands, [2]Department of Electrical Engineering, Mathematics and Computer Science, Delft University of Technology, Delft, Netherlands, [3]Deltares, Delft, Netherlands

Key Points:
- State space methods have been used to study sea level variability in the North Sea.
- Removing known variability increases the accuracy of the estimated decadal variability.
- A low-frequency variability signal is found, which is linked to a steric signal in the Atlantic.

Supporting Information:
- Supporting Information S1

Correspondence to:
T. Frederikse,
t.frederikse@tudelft.nl

Citation:
Frederikse, T., R. Riva, C. Slobbe, T. Broerse, and M. Verlaan (2016), Estimating decadal variability in sea level from tide gauge records: An application to the North Sea, *J. Geophys. Res. Oceans*, *121*, 1529–1545, doi:10.1002/2015JC011174.

Received 27 JUL 2015
Accepted 21 JAN 2016
Accepted article online 2 FEB 2016
Published online 4 MAR 2016

Abstract One of the primary observational data sets of sea level is represented by the tide gauge record. We propose a new method to estimate variability on decadal time scales from tide gauge data by using a state space formulation, which couples the direct observations to a predefined state space model by using a Kalman filter. The model consists of a time-varying trend and seasonal cycle, and variability induced by several physical processes, such as wind, atmospheric pressure changes and teleconnection patterns. This model has two advantages over the classical least-squares method that uses regression to explain variations due to known processes: a seasonal cycle with time-varying phase and amplitude can be estimated, and the trend is allowed to vary over time. This time-varying trend consists of a secular trend and low-frequency variability that is not explained by any other term in the model. As a test case, we have used tide gauge data from stations around the North Sea over the period 1980–2013. We compare a model that only estimates a trend with two models that also remove intra-annual variability: one by means of time series of wind stress and sea level pressure, and one by using a two-dimensional hydrodynamic model. The last two models explain a large part of the variability, which significantly improves the accuracy of the estimated time-varying trend. The best results are obtained with the hydrodynamic model. We find a consistent low-frequency sea level signal in the North Sea, which can be linked to a steric signal over the northeastern part of the Atlantic.

1. Introduction

The tide gauge record represents the main source of information about sea level change during the last two centuries [*Gornitz et al.*, 1982; *Douglas*, 1991]. Available observations are generally accurate and characterized by a dense (subdaily) temporal sampling. However, their local nature in combination with a sparse and uneven spatial distribution largely limits the accuracy of global and regional sea level change estimates [*Woodworth et al.*, 2009].

In an effort to increase the achievable accuracy, many studies have focussed on estimating linear trends of sea level change at secular scales [*Douglas*, 1991; *Holgate*, 2007; *Church and White*, 2011; *Calafat and Chambers*, 2013; *Wenzel and Schröter*, 2014]. Nonetheless, the presence of (multi-)decadal variability can influence estimates of long-term effects [*Dangendorf et al.*, 2014a, 2015], especially if the record is of limited extent: Jordà [2014] argued that, with the known properties of temporally correlated noise in sea level, at least 60 years of data are needed to detect a superposed long-term trend of 2 mm/yr. Moreover, the implicit assumption that the long-term behavior of sea level can be parametrized as a linear or quadratic trend might not be justified on time scales at which significant unexplained variability is present.

We propose a new parametrization of sea level change for individual tide gauge stations, based on a state space formulation. This formulation partitions the signal between a set of processes defined by a prescribed state space model. The processes in our state space model include a time-varying trend, cyclic terms, regressors, and a residual.

The time-varying trend is not bound to a shape that is prescribed a priori, such as a linear or quadratic function: it rather represents the combined effect of secular changes and of variability at scales not captured by other terms in the model. The smoothness of the time-varying trend can be controlled by letting the residual term absorb high-frequency signals. Cyclic terms allow variations in phase and amplitude over time. These variations are mainly driven by variability in the heating and cooling of the ocean, meteorological

forcing, and to a smaller extent by ice and land hydrology processes. Regressors describe the impact of meteorological effects, such as wind and pressure, and of global teleconnection patterns, such as the North Atlantic Oscillation and the Multivariate ENSO index.

State space formulations are widely used in econometrics [*Harvey*, 1990], and have been introduced recently in the geoscience community by *Davis et al*. [2012] and Laine et al. [2014].

Because the time-varying trend captures both the long-term trend as well as variability on decadal scales, the method provides insight in patterns of decadal variability of mean sea level in tide gauge records after the linear effects associated with wind, pressure, and global teleconnection patterns have been filtered out. The time-varying trend will therefore contain the effects of remote atmospheric forcing and large-scale steric and ocean mass effects, which typically show variability on decadal and multidecadal time scales as well as trends related to climate change.

To study the performance of the state space model, time series from tide gauge station around the North Sea have been analyzed. The North Sea is a shallow sea, with an average depth of approximately 90 m, located at the European continental shelf. It has been chosen because it shows variability over a wide range of scales, high quality tide gauge data are available, and it has already been the object of extensive study [*Wahl et al*., 2013]. The barotropic sea level response to wind and pressure changes in the North Sea is significant, and accounts for a large part of the variability [*Dangendorf et al*., 2013, 2014b], although it does not explain variability at decadal scales [*Dangendorf et al*., 2014a]. *Calafat et al*. [2012] have linked the decadal variability along the Western European coast to the cumulative response of the ocean to longshore winds, integrated from the equator to the European coast. This signal has also been observed further North along the Norwegian coast [*Calafat et al*., 2013]. *Dangendorf et al*. [2014b] have shown that the Newlyn tide gauge record, for which the decadal variability is to a large extent linked to the integrated longshore wind, can be used as a proxy for this signal in the North Sea.

Three space state models are compared: the first model consists of a time-varying trend and a residual, the second model also includes cyclic terms and makes use of regressors to reduce the unexplained signal variance, while the third model reduces variance by means of a storm surge model. The storm surge model explicitly solves the depth-integrated equations of motion over the North Sea basin, and provides a more accurate estimate of the influence of the barotropic response of sea level to meteorological processes, compared to a model that uses simple linear regression between wind stress, pressure and sea level.

In section 2, we briefly discuss the theory behind the state space formulation, which is to a great extent based on *Durbin and Koopman* [2012]. In section 3, the three state space models are defined. Results for the North Sea are presented in section 4. Discussion and conclusions can be found in section 5.

2. The State Space Formulation

The state space model uses series of observations to estimate trends, next to other components such as cyclic (seasonal harmonic) signals or correlations with external time series (regression). In contrast to deterministic least squares estimators, it allows trends and other components to vary in time. For the observations $\mathbf{y}=y_1,..,y_n$ (e.g., the sea level observed at a specific tide gauge station) we set up the general structure of our model following *Harvey* [1990] and *Durbin and Koopman* [2012] as:

$$y_i=\mu_i+\sum_j c_{i,j}+\sum_k h_{i,k}+\zeta_i+\epsilon_i \quad \text{for } i=1\ldots n \tag{1}$$

This state space model consists of a trend μ_i, j cycle terms c_i with periods T_{cycle_j}, k regressors h_i and a residual, which consists of two parts: a component ζ_i that follows an autoregressive model and an irregular component ϵ_i, which should be Gaussian distributed. The subscript i denotes the scalar value at time t_i. In most state space literature equations are provided for time series with equally spaced time steps, here we use the so-called continuous time approach, which allows for arbitrarily spaced time steps. With this approach, the sample rate does not have to be constant, so missing observations are automatically taken into account. In state space models each component is defined recursively, such that the trend μ_{i+1} (where μ_i is the level of the trend at time t_i) is an update of μ_i plus a slope times the normalized time step $dt_i=\frac{t_i-t_{i-1}}{\text{mean}(t_i-t_{i-1})}$, with $\text{mean}(t_i-t_{i-1})$ the mean time step size:

$$\mu_{i+1} = \mu_i + v_i dt_i \tag{2}$$

Time variability is introduced by the update of the slope v_i by an added random walk term ξ_i:

$$v_{i+1} = v_i + \xi_i \sqrt{dt_i} \quad \xi_i \sim N(0, \sigma_\xi^2) \tag{3}$$

This results in a trend model which is known in literature as the local trend model or integrated random walk. When we set the variance of the random walk term ξ_i to zero we arrive again at the common deterministic trend model that can be solved in a least squares sense. The cycle term c_i reads in deterministic form as:

$$c_i = \tau \cos(\lambda t_i + \phi) = c\cos(\lambda t_i) + c^* \sin(\lambda t_i) \tag{4}$$

where τ is the amplitude, ϕ the phase offset and $\lambda = \frac{2\pi}{T_{cycle}}$. The cycle term can be written in a recursive form using the cosine and sine addition theorems as [*Harvey*, 1990]:

$$\begin{aligned} c_{i+1} &= c_i \cos(\lambda \cdot dt_i) + c_i^* \sin(\lambda \cdot dt_i) + \omega_i \sqrt{dt_i} \omega_i \sim N(0, \sigma_\omega^2) \\ c_{i+1}^* &= -c_i \sin(\lambda \cdot dt_i) + c_i^* \cos(\lambda \cdot dt_i) + \omega_i^* \sqrt{dt_i} \omega_i^* \sim N(0, \sigma_{\omega^*}^2) \end{aligned} \tag{5}$$

The random walk term ω_i adds time variability to the cycle terms. Phase offset ϕ_i and amplitude τ_i can be calculated from c_i and c_i^* by:

$$\tau_i = \sqrt{c_i^2 + c_i^{*2}} \tag{6}$$

$$\phi_i = -\tan^{-1} \frac{c_i^*}{c_i} - t_i \lambda \mod(2\pi) \tag{7}$$

The contribution h_i of a regressor x_i (the time series of an explanatory variable) with constant regression coefficient β is defined as [*Durbin and Koopman*, 2012]:

$$h_i = \beta x_i \tag{8}$$

The autoregressive part of the residual is modeled as follows [*Harvey*, 1990]:

$$\zeta_i = \phi^{dt_i} \zeta_{i-1} + \psi_i dt_i \quad \psi_i \sim N(0, \sigma_\psi^2) \tag{9}$$

The generalized state space formulation can be written as:

$$y_i = Z_i \alpha_i + \epsilon_i \tag{10}$$

where Z_i is the design matrix, state vector α_i contains the unknowns and again ϵ_i is the residual or irregular component. The updates of the state α_{i+1} are written as:

$$\alpha_{i+1} = T\alpha_i + \eta_i \tag{11}$$

with transition matrix T and a combined disturbance vector η_i that contains all random walk terms of the trend, cycle, and regressor components. In case we define a model including a trend, an annual cycle ($\lambda = 2\pi$), and one regressor, the state space model has a design matrix Z_i and state vector α_i:

$$Z_i = [1 \quad 0 \quad 1 \quad 0 \quad x_i \quad 1] \tag{12}$$

$$\alpha_i = [\mu_i \; v_i \; c_i \; c_i^* \; \beta_i \; \zeta_i]' \tag{13}$$

For this specific model, the transition matrix reads as:

$$T_i = \begin{bmatrix} 1 & dt_i & 0 & 0 & 0 & 0 \\ 0 & 1 & 0 & 0 & 0 & 0 \\ 0 & 0 & \cos(\lambda dt_i) & \sin(\lambda dt_i) & 0 & 0 \\ 0 & 0 & -\sin(\lambda dt_i) & \cos(\lambda dt_i) & 0 & 0 \\ 0 & 0 & 0 & 0 & 1 & 0 \\ 0 & 0 & 0 & 0 & 0 & \phi^{dt_i} \end{bmatrix} \tag{14}$$

The disturbance vector reads:

$$\eta_i = [0\ \xi_i\ \omega_i\ \omega_i^*\ 0\ \psi_i]' \tag{15}$$

2.1. Kalman Filter and Smoother

We use a Kalman filter to recursively estimate the state vector [1 x m] at each time step, using observations $Y = y_1, .., y_i$

$$\mathbf{a}_{i+1} = \mathrm{E}(\alpha_{i+1}|Y) \tag{16}$$

and its error variance [m x m]:

$$P_{i+1} = \mathrm{var}(\alpha_{i+1}|Y) \tag{17}$$

The Kalman filter consists of the following equations for the prediction error v_i with variance F_i. K_i is the Kalman gain. R_i is commonly an identity matrix [e.g., *Durbin and Koopman*, 2012]:

$$v_i = y_i - Z_i\mathbf{a}_i \tag{18}$$

$$F_i = Z_iP_iZ_i' + H_i \tag{19}$$

$$K_i = T_iP_iZ_i'F_i^{-1} \tag{20}$$

We initialize a_1 with 0 and P_1 with a large number (in our case $P_1 = 10^3$). Here H_i [1 x 1] contains the variance of the irregular component:

$$H_i = \sigma_\epsilon^2 dt_i \tag{21}$$

Q [m x m] contains the disturbance variances

$$Q_i = I\sigma_{\eta_i}^2 dt_i \tag{22}$$

These steps are followed by a prediction for the filtered state $\mathbf{a}_{i+1}$ and variance P_{i+1} for the next time step:

$$\mathbf{a}_{i+1} = T_i\mathbf{a}_i + K_iv_i \tag{23}$$

$$P_{i+1} = T_iP_i(T_i - K_iZ_i)' + R_iQ_iR_i' \tag{24}$$

The estimate $\mathbf{a}_i$ of the state α_i improves progressively using information up to $\mathbf{y}_{i-1} = y_1, \ldots, y_{i-1}$. To improve the estimate for the full state, we use a state smoother that provides a smoothed estimate $\hat{\alpha}_i$ of the state α_i and error variance V_t based on all available observations $\mathbf{y} = y_1, .., y_n$:

$$\hat{\alpha}_i = \mathrm{E}(\alpha_i|\mathbf{y}) \tag{25}$$

and its error variance:

$$V_i = \mathrm{var}(\alpha_i|\mathbf{y}) \tag{26}$$

The smoother computes smoothed estimates using the following steps [*De Jong*, 1989; *Durbin and Koopman*, 2012]:

$$L_i = T_i - K_iZ_i \tag{27}$$

$$\mathbf{r}_{i-1} = Z_i'F_i^{-1}v_i + L_i'\mathbf{r}_i \tag{28}$$

$$N_{i-1} = Z_iF_i^{-1}Z_i + L_i'N_iL_i \tag{29}$$

$$\hat{\alpha}_i = \mathbf{a}_i + P_i\mathbf{r}_{i-1} \tag{30}$$

$$V_i = P_i - P_iN_{i-1}P_i \tag{31}$$

with $\mathbf{r}_n$ and N_n equal to 0. An alternative formulation of the smoother computes smoothed estimates of disturbances ϵ_i and η_i:

$$\hat{\epsilon}_i = \mathrm{E}(\epsilon_i|\mathbf{y}) \quad \hat{\eta}_i = \mathrm{E}(\eta_i|\mathbf{y}) \tag{32}$$

These are calculated using the following recursion for $i=n,..1$ by [*Koopman*, 1993; *Durbin and Koopman*, 2012, chap. 4.5]:

$$u_i = F_i^{-1} v_i - K_i' \mathbf{r}_i \tag{33}$$

$$D_i = F_i^{-1} + K_i' N_i K_i \tag{34}$$

$$N_{i-1} = Z_i' D_i Z_i + T'_i N_i - Z_i' K_i' N_i T_i - T_i' N_i K_i Z_i \tag{35}$$

$$r_{i-1} = Z_i' u_i + T_i' \mathbf{r}_i \tag{36}$$

$$\hat{\epsilon}_i = H_i u_i \tag{37}$$

$$\hat{\eta}_i = Q_i R_i' \mathbf{r}_i \tag{38}$$

2.2. Estimation of State Variance, Process Variance, and the Autoregressive Coefficient

Because the variance of the residual σ_ϵ^2 and the variance of the disturbances of each component σ_η^2, as well as the AR parameter ϕ, are unknowns we have to estimate them a priori. We statistically optimize these variances by maximizing the likelihood $\mathcal{L}(\mathbf{y})$ of the data, given the variances of the process noise and disturbance noise, defined as:

$$\mathcal{L}(\mathbf{y}) = \mathrm{p}(y_1, \ldots, y_n | \sigma_\epsilon^2, \sigma_\eta^2, \phi) \tag{39}$$

More specific, the log $\mathcal{L}$ is maximized, which equals [*Schweppe*, 1965; *Durbin and Koopman*, 2012, chap. 7.2]:

$$\log \mathcal{L}(\mathbf{y}) = -\frac{n}{2} \log(2\pi) - \frac{1}{2} \sum_{t=1}^{n} (\log |F_t| + V_t' F_t v_t) \tag{40}$$

For the variance parameters we maximize the log likelihood using the Estimation/Maximization (EM) algorithm [*Shumway and Stoffer*, 1982; *Watson and Engle*, 1983], which iteratively updates the variances by maximizing the log likelihood of the data until convergence has been reached by [*Koopman*, 1993]:

$$\sigma_{\epsilon,\mathrm{new}}^2 = \sigma_{\epsilon,\mathrm{old}}^2 + \sigma_{\epsilon,\mathrm{old}}^2 \frac{1}{n} \sum_{t=1}^{n} \left(u_t^2 - D_t\right) \sigma_{\epsilon,\mathrm{old}}^2 \tag{41}$$

$$\sigma_{\eta,\mathrm{new}} = \sigma_{\eta,\mathrm{old}}^2 + \sigma_{\eta,\mathrm{old}}^2 \frac{1}{n-1} \sum_{t=1}^{n} (\mathbf{r}_{i-1} \mathbf{r}'_{i-1} - N_{i-1}) \sigma_{\eta,\mathrm{old}}^2 \tag{42}$$

This iterative procedure will result in a local maximum of the log likelihood for the process and noise variances, which requires a good initial guess, because more local maxima may be present. The iterations include runs of the Kalman filter and the disturbance filter that provides values for D_i and N_i.

The autoregressive coefficient ϕ is estimated by detecting the maximum of the loglikelihood for ϕ in the domain (0 1).

2.3. Mean Trend and Confidence Intervals

When the integrated random walk term of the trend σ_ξ^2 is nonzero (*equation* (3)), the estimated trend will not have a constant slope. If we nevertheless want to estimate an average trend from the time-varying trend, we can integrate the slope v over the complete time interval Δt. Following equation (2), we obtain

$$\bar{v} = \frac{1}{\Delta t} (\mu_n - \mu_1) \tag{43}$$

The standard deviations of the averaged slope can be derived using standard propagation of uncertainty using the standard deviation of the time variable mean σ_{μ_i} from the smoothed state variance V and autocovariances of the smoothed slope $\sigma_{\mu_{ij}}$.

$$\sigma_{\bar{\nu}} = \frac{1}{\Delta t}\sqrt{\sigma^2_{\mu_1} + \sigma^2_{\mu_n} - 2\sigma_{\mu_{1,n}}} \tag{44}$$

The auto-covariance matrix of the smoothed state ($\sigma_{\mu_{i,j}}$) is defined as [*De Jong*, 1989; *Durbin and Koopman*, 2012, *section 4.7*]:

$$\mathrm{cov}(\hat{\alpha}_i, \hat{\alpha}_j) = P_i L_i' L_{i+1}' \cdots L_{j-1}' (I - N_{j-1} P_j) \quad j \geq i \tag{45}$$

3. Three State Space Models for Regional Sea Level Changes

The available sea level observations at a specific tide gauge location are coupled to the various processes that cause variability by a state space model. The state space model defines the regressors and cycles that are included in the analysis. We use three different state space models: model A estimates a time-varying trend and noise. Model B also includes cycle and regressor terms. Model C is similar to model B, except that model C uses the results from a storm surge model that calculates the barotropic sea level response to wind, atmospheric pressure and tides as a regressor.

3.1. Model A: Time-Varying Trend Only

Model A parametrizes the sea level as a time-varying trend plus a residual:

$$y_i = \mu_i + \zeta_i + \epsilon_i \tag{46}$$

In this equation, y_i are the observations of the sea level at time steps t. μ_i is the time-varying trend, which incorporates the time-mean of the series, the long-term trend and multiannual variability. The residual consists of an autoregressive part ζ_i and an irregular part ϵ_i, and contains variability that is not explained by the other terms is the model.

3.2. Model B: Trend, Cycles, and Regressors

In model B we extend model A by adding cycle terms and regressors. The regressors account for variability in the sea level caused by various known processes. We estimate the sea level as a linear combination of the individual contributions.

Two cycle terms are used in this model: an annual and a semiannual cycle. The annual cycle found in tide gauge records is caused by a sum of effects, including a seasonal cycle in sea water temperature, atmospheric forcing [*Plag and Tsimplis*, 1999], freshwater fluxes from land hydrology, and the tidal constituent SA (Solar Annual) [*Pugh and Woodworth*, 2014]. Since these processes, except for the tidal component, are only approximately represented by a sinusoid, the phase offset and the amplitude of this cycle are treated as stochastic. Therefore, the phase offset and amplitude are allowed to vary over time. The semiannual cycle is caused by the tidal constituent SSA (Solar semiannual), and by a part of the seasonal signal. The amplitude and the phase offset of the half-yearly cycle are also regarded as stochastic. Next to the annual and semiannual tidal cycle, the nodal cycle with a period of 18.6 years is present in the astronomical equilibrium tide, and some authors suggest a significant influence on sea level variability [*Baart et al*., 2011]. To incorporate the effect of the nodal cycle on sea level, it has been added to the list of regressors with a fixed phase offset following the equilibrium law, as suggested by *Proudman* [1960] and Woodworth [2011]:

$$C_{\mathrm{nodal}} = \cos\left(\frac{2\pi(t_i - t_0)}{18.61}\right) \tag{47}$$

where C_{nodal} is the regressor, t_i the time at each time step in years, and t_0 is 1922.7 years. This cycle should produce a positive regression coefficient on latitudes smaller than 35°, and a negative regression coefficient on higher latitudes, according to the equilibrium law.

Next to the nodal tide, regressors account for variability caused by wind stress, atmospheric pressure and variability associated with global teleconnection patterns. For the regressors for wind stress and atmospheric pressure, monthly mean time series have been obtained from ERA-interim, a global reanalysis product [*Dee et al*., 2011]. By selecting the grid points that are within 1° of the station and at sea and taking their average, a monthly time series is constructed. Note that, although the response to wind is not purely local, taking a larger averaging area, for example 4°, does not lead to a significantly different fraction of variance explained. The regressor of pressure represents the inverse barometer effect, so the spatial-mean pressure

over the ocean is calculated for each month, and subtracted from the local pressure, following *Wunsch and Stammer* [1997].

Following *Calafat and Chambers* [2013], we add monthly mean series of three global teleconnection patterns to the list of regressors: the North Atlantic Oscillation (NAO), the Pacific Decadal Oscillation (PDO) and the Multivariate El Niño-Southern Oscillation index (MEI). The NAO measures the differences in the anomalies of the sea level pressure between subtropical and Arctic regions in the Atlantic Ocean [*Hurrell et al.*, 2003]. The PDO is defined by anomalies of ocean water temperatures in Pacific Ocean [*Mantua et al.*, 1997]. The MEI represents the variability caused by El Niño events [*Wolter and Timlin*, 1993].

For each station, the significance of the correlation between each regressor and the observed sea level is calculated. Only regressors with a significant correlation are used in the state space model for a specific station, which is enforced by only accepting regressors with a p-value smaller than 0.01, which corresponds to a significance at the 99% level.

We also require that each regressor solves a specific part of the variance that is independent from other regressors. This requirement is tested by adding the regressors stepwise into a least-squares model with an intercept, linear trend, and cycles without varying phase offset and amplitude, starting with the regressor that has the highest correlation with the sea level. Each regressor is only allowed when the regression coefficient is significant at the 95% level, which is determined using t-statistics. If all regressors are included, the model reads:

$$\begin{aligned} y_i = {} & \mu_i + a_{1,i}\cos\left(2\pi f_1 t_i + \phi_{1,i}\right) + a_{2,i}\cos\left(2\pi f_2 t_i + \phi_{2,i}\right) \\ & + b_1 \cdot u_{\text{wind}} + b_2 \cdot v_{\text{wind}} + b_3 \cdot (p - p_0) \\ & + c_1 \cdot \text{NAO} + c_2 \cdot \text{MEI} + c_3 \cdot \text{PDO} \\ & + d \cdot C_{\text{nodal}} + \zeta_i + \epsilon_i \end{aligned} \tag{48}$$

The annual cycle term is represented by $a_{1,i}\cos\left(2\pi f_1 t_i + \phi_{1,i}\right)$, with $a_{1,i}$ the time-varying amplitude, fixed frequency $f_1 = 1y^{-1}$ and time-varying phase offset $\phi_{1,i}$. The term $a_{2,i}\cos\left(2\pi f_2 t_i + \phi_{2,i}\right)$ represents the semiannual cycle, also with a stochastic amplitude and phase offset. The cycle terms are implemented as in equation (5). The terms u_{wind}, v_{wind} are time series of the local zonal and meridional wind stress. p is the local pressure and p_0 is the monthly mean pressure over all oceans. The terms NAO, MEI, and PDO represent time series of the teleconnection patterns mentioned before. The term C_{nodal} represents the nodal cycle. The time-varying unknowns that are estimated by the state space formulation are μ, a_1, ϕ_1, a_2 and ϕ_2. The unknowns b_1, b_2, b_3, c_1, c_2, c_3, and d are also estimated by the state space formulation, but they are not allowed to vary over time.

3.3. Model C: Corrections From a Storm Surge Model

In model C, the barotropic response of the sea level to atmospheric and tidal forces is modeled using the Dutch Continental Shelf Model (DCSM) version 6. The modeled time series of the sea level height at the grid point closest to the tide gauge is subsequently added as a regressor. When adding the modeled water height as a regressor, rather than subtracting it from the observed water level, the uncertainty of the fitting parameter is taken into account in the error analysis of the state space model. DCSM v6 [*Zijl et al.*, 2013] is a two-dimensional hydrodynamic model that solves the depth-integrated shallow water equations over the North Sea continental shelf, ranging from 15° W to 13° E and from 43° N to 64° N with a horizontal grid spacing of about $1/40°$ in the east-west direction and $1/60°$ in the north-south-direction, which leads to a grid cell length of about 1 nautical mile. The model has been developed to forecast storm surge heights along the North Sea coast. The vertical boundaries are forced with wind stress at the top, and surface friction at the bottom. The horizontal boundaries are closed using a no-normal-flow condition at coastal boundaries. At the open boundaries, the sea surface height is prescribed, which is calculated from astronomical tides, the inverse barometer effect and mean sea level. Next to the diurnal and semidiurnal tides, the long-period tidal constituents SSA (period of 182.6 days), MM (27.6 days), MSF (14.8 days), MF (13.7 days) and MTM (9.2 days) are prescribed. The inverse barometer correction is calculated from ERA-interim before 1993, and from MOG2D [*Carrère and Lyard*, 2003] afterward. The surface drag coefficient has also been obtained from ERA-interim.

The use of a hydrodynamic model has the advantage over the method with regressors for wind and pressure, that nonlinear effects are taken into account, and that the interaction between tides and surges is explicitly solved.

Because the model is barotropic, height variations due to sea water temperature and salinity changes are still present in the signal after removing the modeled sea level, including the part of the seasonal cycle that is caused by steric effects. Furthermore, the long-term constituents SA and the nodal cycle are not forced at the boundaries. Hence, a stochastic annual and semiannual cycle are added to the state space model, together with the nodal cycle term.

The teleconnection patterns NAO, PDO and MEI are also added as a regressor. Each regressor is tested for significance using stepwise addition. If all terms are significant, model C reads:

$$\begin{aligned} y_i = \mu_i + a_{1,i}\cos(2\pi f_1 t_i + \phi_{1,i}) + a_{2,i}\cos(2\pi f_2 t_i + \phi_{2,i}) \\ + b \cdot y_{\mathrm{DCSM}} + c_1 \cdot \mathrm{NAO} + c_2 \cdot \mathrm{MEI} + c_3 \cdot \mathrm{PDO} \\ + d \cdot C_{\mathrm{nodal}} + \zeta_i + \epsilon_i \end{aligned} \tag{49}$$

where y_{DCSM} is the modeled water height at the specific tide gauge station.

3.4. Linear Least Squares Models

In order to better evaluate the behavior of the state space models, we have also analyzed three models that can be solved by linear least squares. In models AL, BL, and CL, the time-varying trend μ_i is replaced by a linear trend and a bias, and the cyclic terms (in BL and CL) are not stochastic. The regressors are the same as in the corresponding state space models.

4. Results and Discussion for the North Sea

The three state space models have been applied to tide gauges surrounding the North Sea. 17 tide gauge stations have been selected that meet the criterion for data availability of more than 75% during the interval 1980–2013. The stations, with their identification number, are depicted in Figure 1. The time span has been chosen to match the period for which ERA-interim reanalysis data are available, which is used as source for the regressor time series of wind and pressure and serves as input for DCSM. Furthermore, the series are long enough to capture at least one full nodal cycle. Monthly mean sea level data have been obtained from the Permanent Service for Mean Sea Level [*Holgate et al*., 2012]. All heights are relative to the PSMSL Revised Local Reference datum. For the Cuxhaven tide gauge, time series that are corrected for the conversion between mean sea level and mean tide level are used, following the method of *Wahl et al*. [2011].

4.1. Choice of the Variance Parameters

The choice of the disturbance variance parameters σ_ϵ^2 and σ_η^2 in the state space formulation has an influence on the final result. The disturbance variance parameters of the cycle terms and the irregular component are determined using the EM-algorithm, as described in section 2.2. The initial values for the disturbance variance terms σ_η^2 are low, which ensures that when a local maximum of the loglikelihood is found, the variance in the parameters will not be overestimated. An overestimation could lead to the absorption of nonseasonal signals into the cycle terms. To make sure that the time-varying trend consists of long-term variations and variability on scales longer than a few years, the slope disturbance variance parameter is fixed, and a constant value is used for all stations. The slope disturbance variance parameter has been chosen in such a way that variability on decadal and longer scales is represented by the time-varying trend, while variability on shorter time scales that is not explained by the cycle and regressor terms will be captured by the residual term. The time-varying trends calculated using various values of the slope disturbance variance parameter for stations Wick and Hoek van Holland are shown in Figure 2, together with the Power Spectral Densities (PSD's) of the time-varying trends. The figure shows that for a higher slope disturbance variance parameter, details at shorter time scales are revealed. Since for this study, we are interested in variability on decadal and longer scales, and higher disturbance variance parameters cause larger confidence intervals, we choose a slope variance parameter of 2 $\mathrm{mm}^2/\mathrm{yr}^3$ for model C. With this value the time-varying trend shows almost no subdecadal variability, but still captures the decadal variability. The PSD's

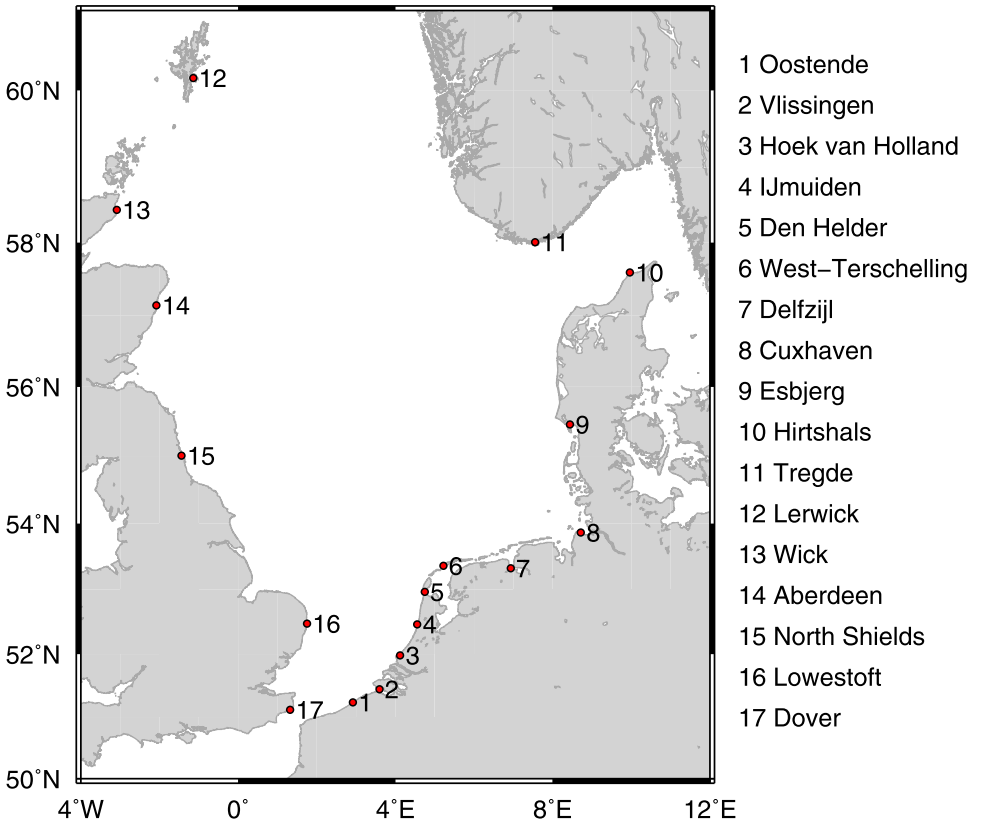

Figure 1. Location of the 17 tide gauge stations around the North Sea.

(right panel of the same figure) quantitatively show that the signals on time scales of 10 years and longer are preserved, while short-term variability on time scales of 7 years and lower is removed for the chosen slope variance parameter. For model B, we use the same value for the slope disturbance variance parameter, because the same range of signals are captured in the time-varying trend. For model A, a parameter of 20 mm^2/yr^3 is used, for which μ contains signals in the same frequency range as in model B and C.

To check whether the choice of the slope disturbance variance parameter influences the estimate of the regression coefficients and the phase and amplitude of the cycle terms, we have calculated the relative standard deviation of these numbers over the range of parameters in Figure 2. All relative standard deviations are smaller than 1%, which shows that the influence of the slope disturbance variance parameter on the estimation of the regression coefficients and cycle terms is low.

4.2. Model Comparison

The time-varying trends $\mu(t)$, with the 68% confidence interval from model A, B, and C for the stations Hoek van Holland, Cuxhaven, Wick and Lowestoft are shown in Figure 3. The picture also shows the 8 year moving average of the trend plus residual for models BL and CL. Moving average filters are commonly used to analyze inter-annual and decadal variability in sea level. The filter width of 8 years is chosen to match the frequency response of the state space filter, that has a cut-off frequency at about 8 years. For all stations, the confidence interval of the time-varying trend for the three state space models overlap. Oscillating patterns on decadal time scales are visible in all three models, and the found patterns are very similar between the three models. The oscillatory pattern of model C does not differ significantly from the pattern of model B and A, except for the first and last few months of the series, where the confidence intervals are large. Models B and C have a much smaller confidence interval for all 4 stations than model A, and therefore, we will focus on models B and C in the next sections.

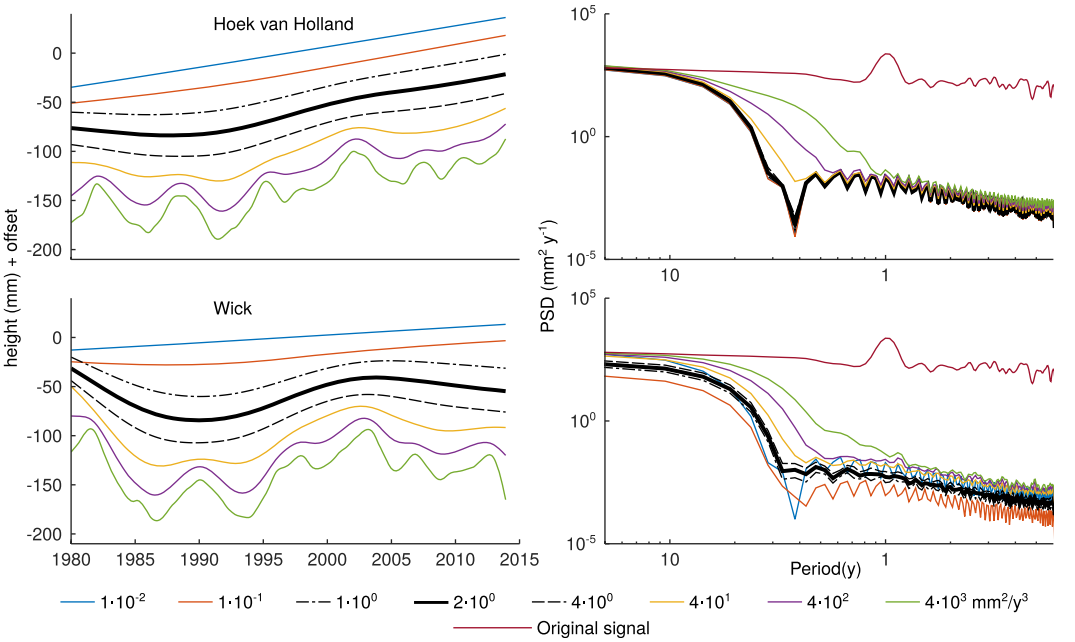

Figure 2. (left) Time-varying trend for different values for the slope disturbance variance parameter for the stations Terschelling and Wick using model C. (right) Power Spectral Density (PSD) of the time-varying trend and the original time series. Welch's method has been used to estimate the PSD.

The moving averages from models BL and CL show a similar pattern of variability, although some high-frequency signals remain visible. There are however differences visible between the patterns of BL and CL, especially for Cuxhaven and Wick. Models B and C show a similar pattern at these stations. Moreover, models B and C do not require data interpolation, and the confidence intervals, computed using the full variance-covariance structure, provide insight into the significance of the oscillations.

To ensure the correct functioning of the state space method, two additional requirements have to be fulfilled: the irregular part of the residuals has to follow a Gaussian distribution, and should not exhibit serial correlation. The first requirement is tested using a Kolmogorov-Smirnov test. On the 95%-level, none of the stations fail the test for model B, three for model C, but eight for model A. Therefore, the estimates of the formal errors for model A might be inaccurate. The second requirement is tested by calculating the lag-n-autocorrelation, with $n=1..120$, which covers the variability at time scales that are not captured by the time-varying trend. The resulting autocorrelation functions for the four mentioned stations are shown in Figure 4. From the plot it can be seen that the irregular component does not show a statistically significant autocorrelation over the tested period.

The individual terms contributing to the signal of models B and C for Hoek van Holland are depicted in Figure 5. The residual of model C is clearly smaller than the residual of model B, which is due to the fact that DCSM is able to simulate the barotropic response to wind more accurately than the regressor model. Also note that at Hoek van Holland, the phase and amplitude of the seasonal cycle do not show large variations with time.

4.3. Patterns of Decadal Variability in the North Sea

With the state space method we can show decadal sea level variability at each tide gauge station. Hence, analyzing the time-varying trend obtained from the state space models allows to look for common patterns of decadal variability. The time-varying trends from model B and C for all stations are shown in Figure 6. Almost all stations show similar behavior: the highest rates of sea level rise are found between 1995 and 2005, while after 2005 rates are much lower and for some stations even negative.

The inflection point around 2005 corresponds to a peak in the nodal cycle [*Woodworth*, 2011; *Pugh and Woodworth*, 2014]. In both state space models, the nodal cycle is present as possible regressor, which allows us to test whether the nodal cycle is responsible for the 2005 inflection point. We find for all stations a

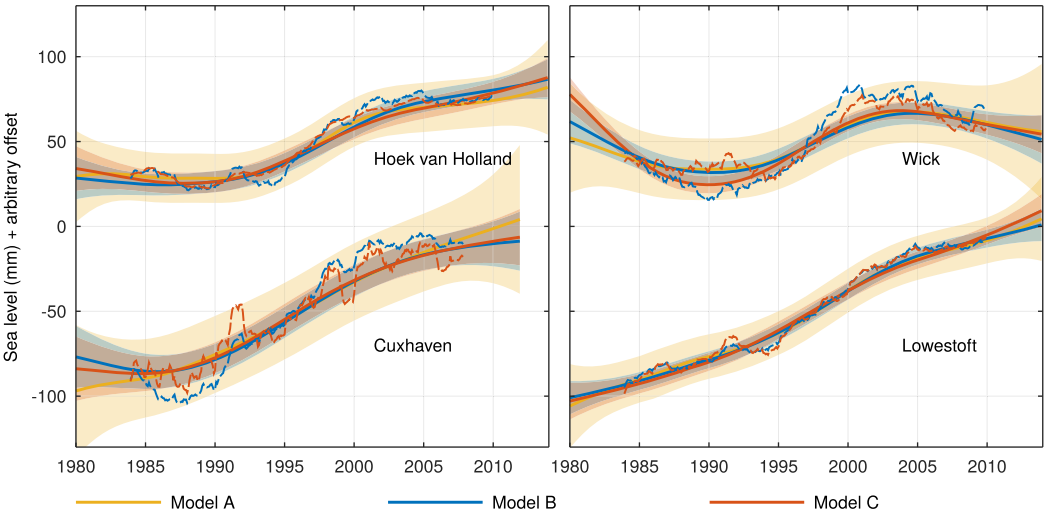

Figure 3. Trends and 68%-level confidence intervals for state space models A, B, and C. The dashed line denotes the 8 year moving average of the trend and residual of models BL and CL.

slightly negative correlation between the sea level height and the nodal cycle. The negative correlation is expected, since all stations lie outside the 35°-zone, for which the astronomical amplitude of the nodal cycle given in equation (47) should be negative. However, on average the correlation coefficient between sea level and the regressor of the nodal tide is very low (−0.07). For all stations, except Aberdeen, for which a cycle with an amplitude of 25 mm was found, the correlation is not significant, according to *p*-statistics on a 95% level. This means that the deceleration after 2005 cannot be linked to the nodal cycle. Furthermore, according to the tidal equilibrium law, the nodal cycle in the North Sea has an amplitude of about 6 mm, considerably lower than the typical amplitude of the found variability, which is in the order of 20 mm. It is unlikely that the phase and amplitude of the nodal cycle would depart significantly from the equilibrium tide [*Woodworth*, 2011]. The significant cycle in Aberdeen has an amplitude four times as large as the equilibrium value. Hence, the correlation is likely not caused by the nodal tide, but to a process with variability at a comparable temporal scale. Therefore, the nodal cycle is not used as a regressor.

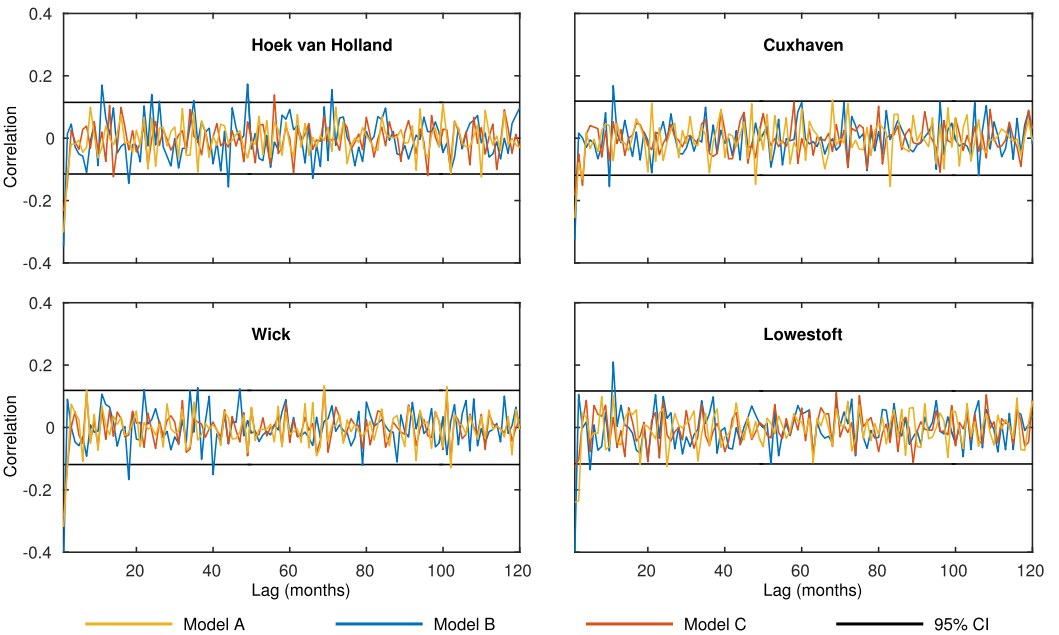

Figure 4. Lag autocorrelation of the irregular component for model A, B, and C. The black line represents the threshold for a significant correlation on the 95%-level.

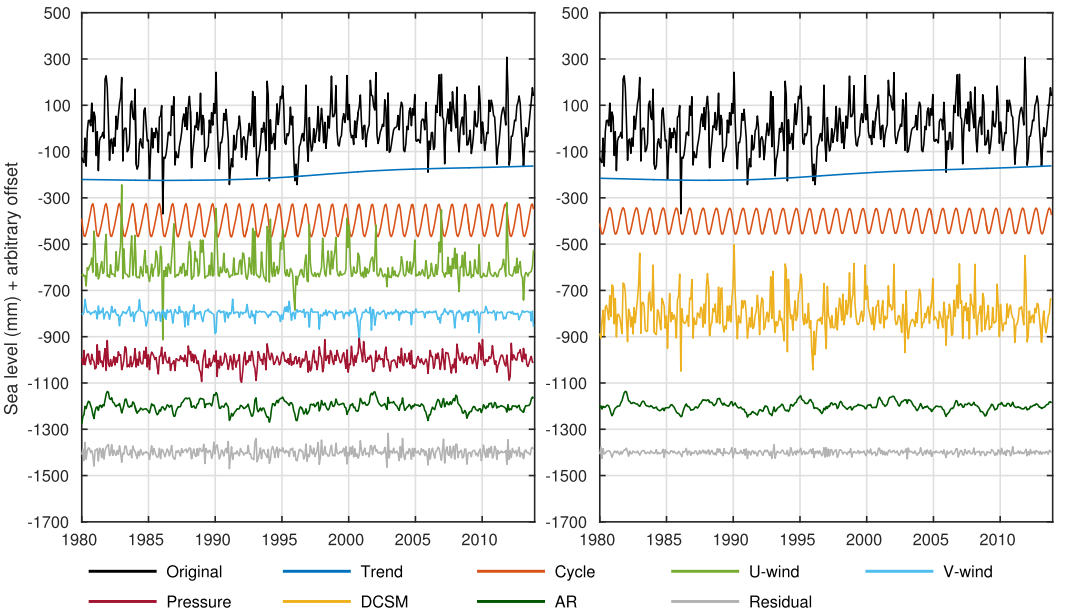

Figure 5. Individual components of the state space model (left) B and(right) C for Hoek van Holland.

The correlation of monthly and yearly tide gauge data between different North Sea stations is well-known [*Wahl et al.*, 2013]. In order to explicitly show similarities in the decadal variability over the whole North Sea, the correlation coefficient between the time-varying trends of all stations is calculated and shown in Figure 7. To prevent correlations due to long-term sea level rise, the correlation coefficient has been calculated after removing the integrated trend. We also show the correlation coefficients of the original sea level data, after removing a linear trend and seasonal cycle. The correlations are shown in Figure 7. To determine the threshold for significance, the number of degrees of freedom is reduced to 5. The latter is based on an 8 year low-pass filter. This number of degrees of freedom leads to a threshold for significance of 0.76 on the 95% level. The figure shows that most stations show a significant positive correlation of the time-varying trend with all

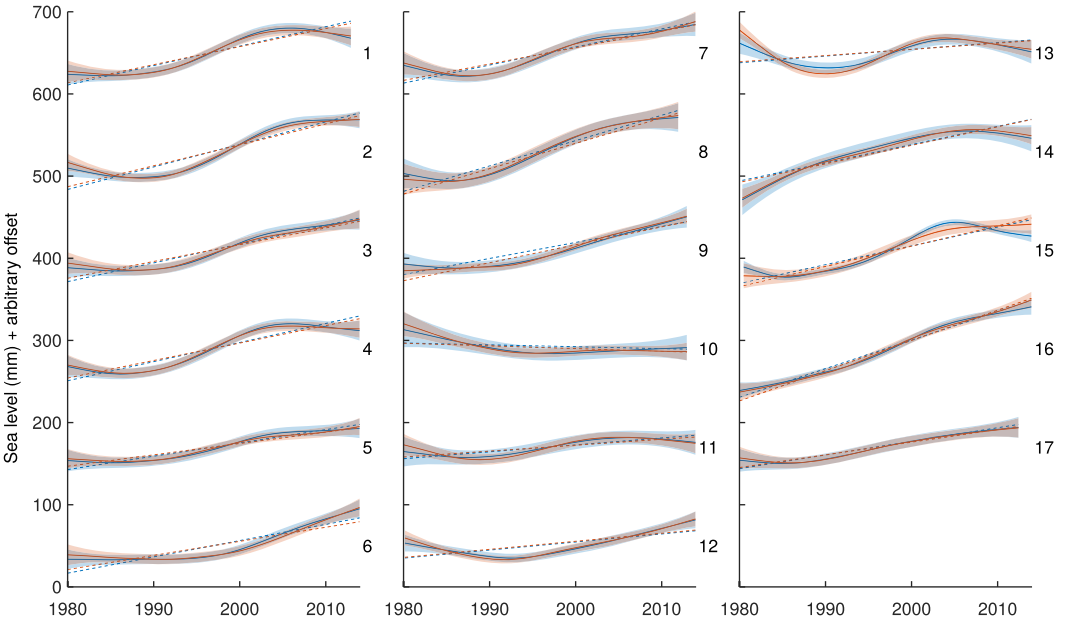

Figure 6. The time-varying trend calculated for model B (blue) and C (yellow) for all stations. The shaded area is the confidence interval for the time-varying trend at the 68% level. The dashed lines depict the linear trend from models BL and CL. The station numbers are according to Figure 1.

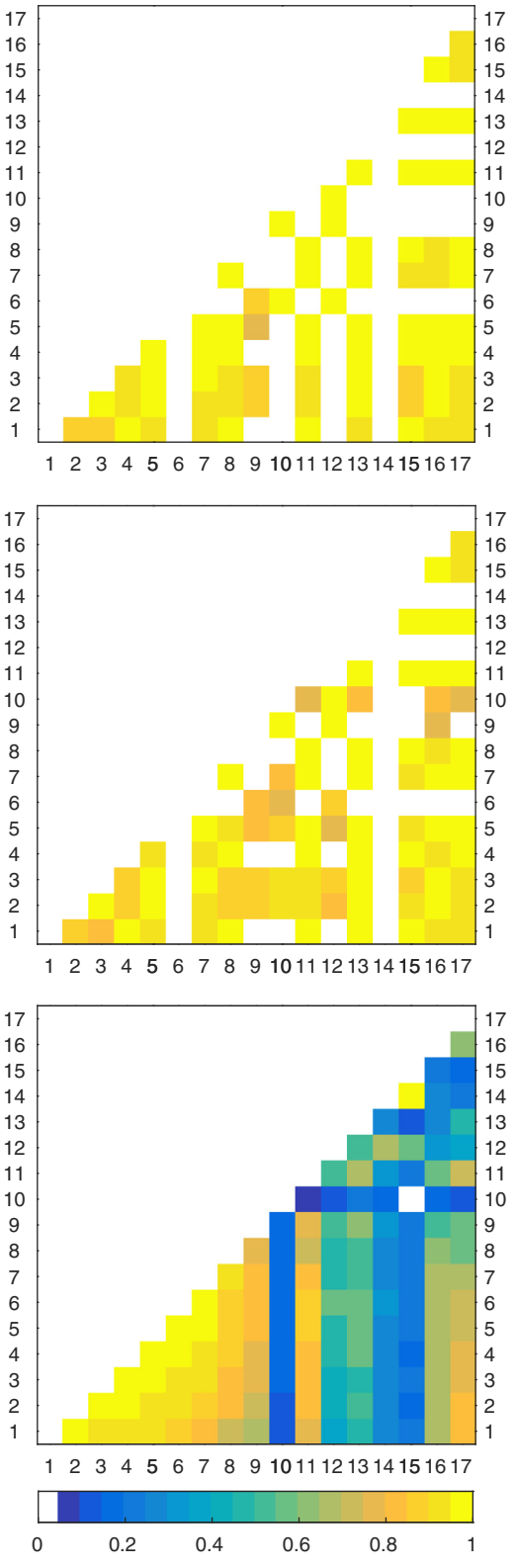

Figure 7. Correlation coefficient between de-trended time-varying trends from different stations for (top) model B, (middle) model C, and (bottom) deseasonalized original data. Correlations that are lower than 0 or insignificant on the 95% level are blank. The stations are numbered according to Figure 1.

other stations. The stations in the southern corner show a very high correlation, both on the Dutch and Belgian coast (stations 1–5) as well as the stations on the English coast (stations 15, 16, 17). The stations at the Wadden Sea (6,7) and in the German Bight (7,8,9) are not as strongly correlated with the southern stations.

Some stations show no significant correlation with any other station: station 14 (Aberdeen) does not show any significant correlation with other, even adjacent, stations. Also station 6 (Terschelling) has generally low correlations with almost all other stations. The German Bight consist of many shallow seas that are subject to rapid changes in bathymetry and current patterns, which could explain the regional differences and the relatively low mutual correlation of decadal sea level variability.

When we compare between the correlations of the time-varying trend and the original data, a different pattern can be seen. For example, the correlation between original data from stations along the Dutch coast show low correlation with stations in northern Great Britain (stations 12–15), while for the time-varying trend this correlation is higher. This difference shows the presence of a basin-wide signal of variability on decadal scales, which cannot be found without removing variability from known processes.

4.4. Sources of Variability

Model B and C explain a large part of the variability in tide gauge observations, which leads to an improved estimate of the sea level variability on decadal time scales that is unexplained by the regressors. The portion of the variability that is solved for each regressor is not equal for all stations. Figure 8 shows the root mean square of the individual variance terms for both models at each tide gauge station. Note that the total explained variance and the variance of the residual do not add up to the total observed variance, because the regressors and cycle terms are not mutually uncorrelated. A table with all regression coefficients is included in the supporting information. For model B, a clear division can be seen between the stations along the south-eastern coast (1–9) and the stations at the British Isles (12–17): the stations along the south-eastern coast show a high total variance, with a peak at the stations in the German Bight (stations 7,8,9). The barotropic response to wind is one of the main contributors to this high variance, and model B and C explain a major part of this

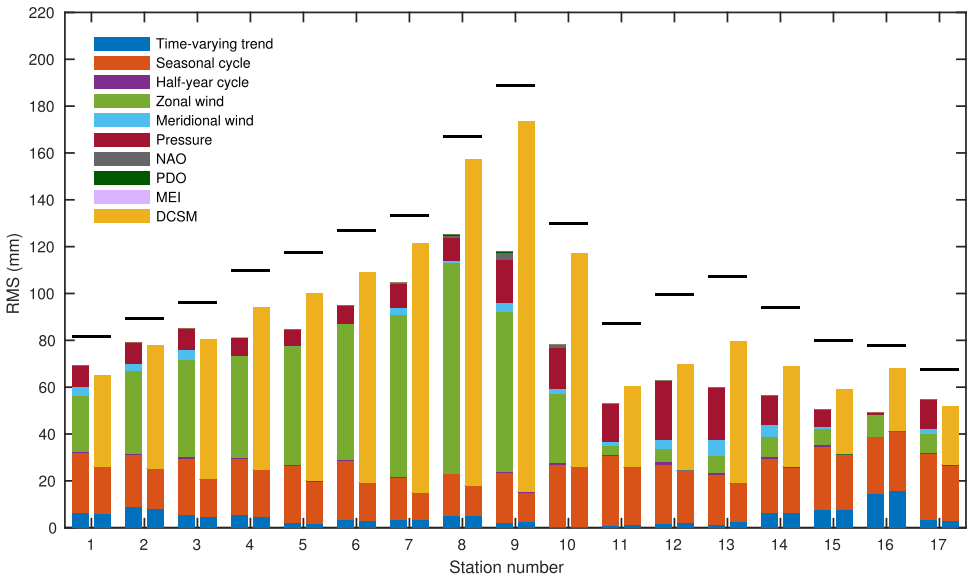

Figure 8. Total and explained variance per individual component: the black bar shows the variance of the observed sea level for each station, and the bar shows the variance of the individual components. For each station, the left bar represents model B, and the right bar model C.

variability. Along the British Isles, the total variance is lower, and the influence of wind is small. For all stations, the regressors for the teleconnection patterns only explain a small fraction of the variance, because the influence of the teleconnection patterns on sea level is driven to a great extent by wind and pressure [*Dangendorf et al.*, 2013].

For all stations, the root mean square error (RMSE) of the residual from model C is smaller than the residual from model B. On average, the RMSE is 45% smaller for model C, compared to model B. Due to the larger fraction of the variance that can be explained, the confidence interval for the time-varying trend is smaller for model C than for model B. Although the typical time scale of the explained variance, which is largely atmosphere-forced, lies below 10 years [*Dangendorf et al.*, 2014b], models B and C show a smaller confidence interval for the time-varying trend than model A.

Calafat et al. [2012, 2013] showed the existence of a consistent pattern of decadal variability along the European and Norwegian coast and linked the pattern to the integrated longshore wind. *Dangendorf et al.* [2014b] argue that the longshore wind signal propagates into the North Sea. They use Newlyn as a proxy for this effect and show that the combination of the Newlyn tide gauge record and remote steric forcing can explain a large part of the decadal variability in the North Sea. However, the coherent time-varying trend signal found here shows variability at longer time scales than the aforementioned studies, so the source of this variability may be different. Since the North Sea is located on a shallow continental shelf, no large local steric effect is expected. Nonetheless, remote steric changes over the much deeper North Atlantic will induce a flow of water over the shelf, affecting local sea level [*Landerer et al.*, 2007]. To determine whether the found pattern in the time-varying trend can be linked to remote steric forcing, the correlation between the time-varying trend of the sea level at the tide gauge stations and steric height over the North Atlantic is calculated. We use the yearly mean steric height from the Ishii & Kimoto data set [*Ishii and Kimoto*, 2009] to calculate a time-varying trend in the steric signal using state space model A. Figure 9 shows that a large region covering the northeast Atlantic has a clear and positive correlation with the time varying trend at the North Sea stations. This finding supports the hypothesis that the observed low-frequency sea level variability in the North Sea can be linked to a large-scale steric signal in the North Atlantic.

4.5. Average Trends

By using equation (43) we can calculate average trends from the state space model, and compare them with the results from the traditional least squares approach. The average time-varying trend contains the

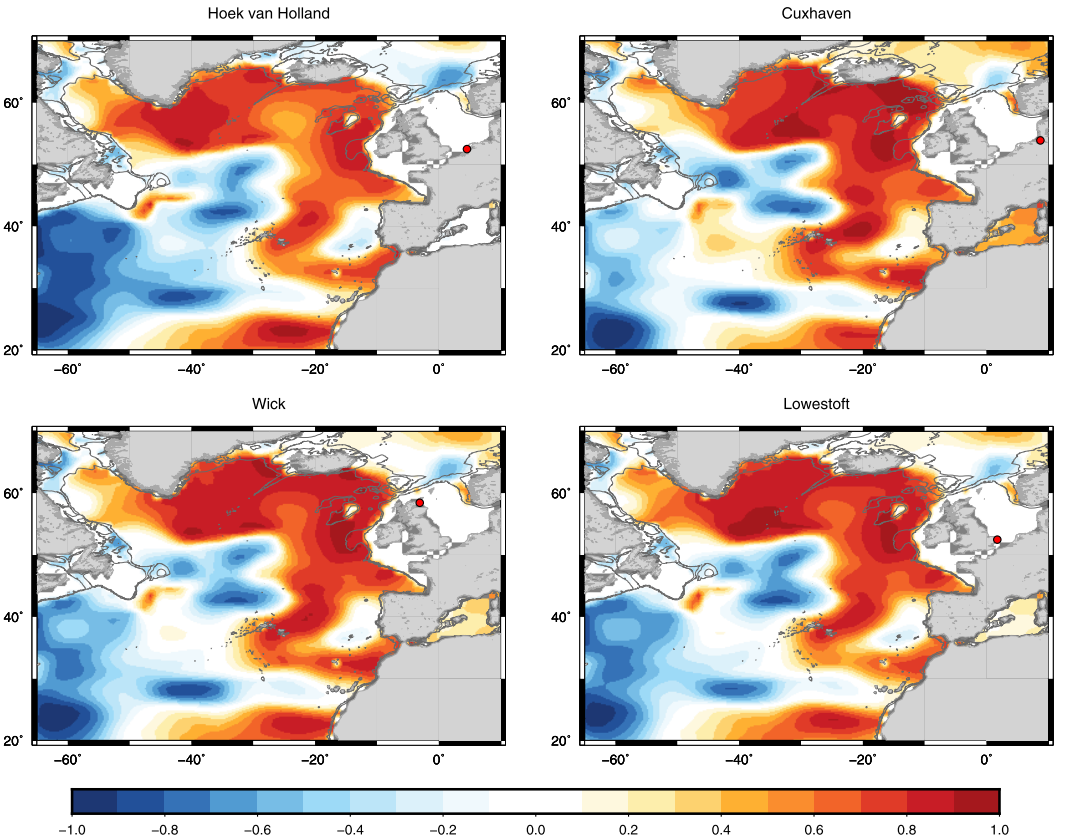

Figure 9. Correlation between time-varying trend in steric sea level and the time-varying sea level trend from model C for four North Sea stations. The 250 and 1000 m isobaths are shown in grey. No correlation is shown for grid points at a depth smaller than 250 m. The averaged time-varying trend for each station and each grid point has been removed using equation (43).

long-term secular trend as well as decadal variability, and does not rely on the assumption that the trend follows a linear path. Table 1 shows the mean trends calculated by the three state space models, as well as the accompanying least squares solutions for all stations. The confidence intervals for the state space models are calculated according to equation (44). For the least-squares fit, the confidence interval has been

Table 1. Mean Trends and Confidence Intervals (at 68% Level) Estimated for All North Sea Stations for All Least Squares Models (AL, BL, CL) and State Space Models (A, B, C)[a]

Station	AL	BL	CL	Model A	Model B	Model C
Oostende	2.3 ± 0.4	2.4 ± 0.2	2.2 ± 0.2	1.4 ± 1.1	**1.3**±0.5	**1.3**±0.5
Vlissingen	2.4 ± 0.5	2.7 ± 0.2	2.5 ± 0.1	1.5 ± 1.0	**1.7**±0.4	**1.5**±0.4
Hoek van Holland	1.9 ± 0.5	2.3 ± 0.2	2.0 ± 0.1	1.5 ± 1.1	1.7 ± 0.5	1.6 ± 0.5
IJmuiden	1.9 ± 0.6	2.3 ± 0.2	2.1 ± 0.1	1.2 ± 1.3	**1.3**±0.5	**1.3**±0.5
Den Helder	1.1 ± 0.6	1.6 ± 0.2	1.4 ± 0.1	1.3 ± 1.4	1.2 ± 0.5	1.2 ± 0.5
Terschelling	1.5 ± 0.7	2.0 ± 0.2	1.7 ± 0.1	2.2 ± 1.5	1.8 ± 0.5	1.7 ± 0.5
Delfzijl	1.6 ± 0.7	2.2 ± 0.3	2.0 ± 0.2	1.5 ± 1.4	1.5 ± 0.6	1.5 ± 0.6
Cuxhaven	3.0 ± 1.0	3.1 ± 0.4	3.1 ± 0.2	3.2 ± 1.8	2.1 ± 0.8	2.4 ± 0.8
Esbjerg	1.9 ± 1.1	1.9 ± 0.4	2.2 ± 0.2	2.8 ± 1.9	1.8 ± 0.6	2.0 ± 0.4
Hirtshals	−0.1±0.8	−0.2±0.3	−0.3±0.2	0.7 ± 1.6	−0.7±0.8	−1.0±0.5
Tregde	0.8 ± 0.5	0.8 ± 0.2	0.7 ± 0.2	0.7 ± 1.3	0.3 ± 0.7	0.1 ± 0.5
Lerwick	1.3 ± 0.6	1.0 ± 0.2	1.0 ± 0.2	2.0 ± 1.4	0.9 ± 0.4	0.7 ± 0.4
Wick	1.0 ± 0.6	0.8 ± 0.2	0.8 ± 0.2	0.1 ± 1.5	**−0.3**±0.6	**−0.7**±0.4
Aberdeen	2.1 ± 0.5	2.2 ± 0.2	2.3 ± 0.2	2.1 ± 1.3	2.2 ± 0.7	2.3 ± 0.5
North Shields	2.2 ± 0.4	2.3 ± 0.2	2.5 ± 0.2	1.7 ± 1.2	**1.1**±0.3	1.9 ± 0.6
Lowestoft	3.4 ± 0.4	3.5 ± 0.2	3.7 ± 0.2	3.3 ± 1.0	3.0 ± 0.4	3.3 ± 0.4
Dover	1.5 ± 0.4	1.7 ± 0.2	1.5 ± 0.1	0.6 ± 1.0	1.2 ± 0.6	1.1 ± 0.6

[a]Bold values denote trends for which the confidence interval of the state space model and the accompanying linear model do not overlap.

corrected for serial correlation by reducing the number of degrees of freedom, according to the procedure described in *Nerem and Mitchum* [2002]. All the confidence intervals are calculated at the 68% confidence level.

At a number of stations, the average time-varying trend is statistically different (at the 68% level) from the least squares trend. Variability on decadal scales is responsible for this difference, by leaking into the estimate of a long-term linear trend. In Figure 3 it can be seen that the variability has a low phase roughly between 1985 and 1995, and a high phase between 1995 and 2010, which causes a positive bias on the estimate of a linear trend. Therefore, linear trends estimated from 30 to 40 years of tide gauge data do not only represent a long-term trend, but also a bias due to decadal variability.

The averaged trends for the three state space models show that the trends found by model B and C lie within the confidence interval of the trend from model A for all stations. The average trends of model B and C are also very similar: there are no stations for which the confidence intervals do not overlap. Of the three state space models, model C shows the smallest confidence interval, averaged over all stations. The explanation of variability caused by the various meteorological components of models B and C, leads to a significant improvement of the accuracy of the estimated trend, compared to the estimation without explaining the various variance terms (model A).

5. Conclusions

We have introduced a new parametrization for time series of observed sea level that takes the presence of unexplained variability on decadal and multidecadal scales into account, which does not rely on the assumption that the underlying long-term trend is linear or quadratic. The time-varying trend captures long-term trends in sea level, as well as variability on decadal and multidecadal scales. Three state space models have been compared using tide gauge data from stations around the North Sea over the period 1980–2013. It is shown that the removal of variance caused by known processes, including the barotropic response to wind and atmospheric pressure changes, contributes to the disclosure of unexplained variability: the state space models that explain parts of the variability perform significantly better than a model that only estimates a long-term trend and a residual. Explaining variance does not only reduce the confidence interval for the estimated time-varying trend, but also reveals an oscillating pattern in sea level on decadal scales. Two models have been compared that remove the variance: one uses regressors from global reanalysis databases, and one uses DCSM, a two-dimensional shallow-water model that calculates sea level changes due to wind, atmospheric pressure and tides. The model that uses DCSM is able to explain a larger part of the variance and estimates a time-varying trend with a smaller confidence interval, compared to the model that uses regressors. The advantage of the model that uses regressors from global reanalysis products, is that it can be used globally, opposed to the DCSM model, which only provides data for the North Sea.

The time-varying trends in sea level for the stations around the North Sea show oscillations, that are consistent over the full basin, although the variability patterns caused by wind and pressure differ between stations. The sea level shows a steep rise between 1995 and 2005, followed by a slowdown between 2005 and 2013. The removal of atmospheric effects either by a simple linear regression or by a barotropic storm surge model reduces the uncertainty in the time-varying trend to an extent that the amplitude of the resulting decadal pattern is larger than the confidence interval of the time-varying trend. It is found that the pattern is not caused by the nodal cycle, but can be linked to a large-scale steric signal that covers the Northeastern part of the Atlantic ocean.

The presence of low-frequency variability influences the estimation of linear trends over short intervals, even after removing the barotropic response to wind and pressure. Variability on decadal (and multidecadal) scales that can not be linked to individual processes leaks into the estimate of a long term linear trend when the length of the analyzed sea level record has a length of the same order as the typical time scale of unexplained variance. Furthermore, there is no reason to expect that on (multi-)decadal time scales, sea level is rising along a linear or quadratic path. In order to find the long-term behavior of sea level, the processes that cause the variability and long-term trend have to be understood.

Acknowledgments
The tide gauge data have been obtained from www.psmsl.org. The indices for the NAO and the PDO have been obtained from NOAA climate prediction center (www.cpc.ncep.noaa.gov/products/precip/CWlink/daily_ao_index/teleconnections.shtml). The MEI has been obtained from NOAA's Earth System Research Laboratory (www.esrl.noaa.gov/psd/enso/mei). ERA-interim reanalysis data have been obtained from ECMWF (www.ecmwf.int/en/forecasts/datasets/era-interim-dataset-january-1979-present). The steric data set from Ishii and Kimoto has been obtained from NCAR (http://rda.ucar.edu/datasets/ds285.3/). We would like to thank Sönke Dangendorf for providing corrected tide gauge data from Cuxhaven. This study was funded through the Netherlands Organisation for Scientific Research (NWO) VIDI grant 864.12.012. Cornelis Slobbe wants to acknowledge financial support by the STW Technology Foundation in The Netherlands (Vertical Reference Frame for the Netherlands Mainland, Wadden Island and Continental Shelf (NEVREF) project, project number 12553). Taco Broerse acknowledges financial support from the SRON/NWO grant GO-AO/20. Furthermore, we would like to thank Sönke Dangendorf and an anonymous reviewer for their valuable comments.

References

Baart, F., P. H. Van Gelder, J. De Ronde, M. Van Koningsveld, and B. Wouters (2011), The effect of the 18.6-year lunar nodal cycle on regional sea-level rise estimates, *J. Coastal Res.*, *28*(2), 511–516.

Calafat, F., and D. Chambers (2013), Quantifying recent acceleration in sea level unrelated to internal climate variability, *Geophys. Res. Lett.*, *40*, 3661–3666, doi:10.1002/grl.50731.

Calafat, F., D. Chambers, and M. Tsimplis (2012), Mechanisms of decadal sea level variability in the eastern North Atlantic and the Mediterranean Sea, *J. Geophys. Res.*, *117*, C09022, doi:10.1029/2012JC008285.

Calafat, F., D. Chambers, and M. Tsimplis (2013), Inter-annual to decadal sea-level variability in the coastal zones of the Norwegian and Siberian seas: The role of atmospheric forcing, *J. Geophys. Res. Oceans*, *118*, 1287–1301, doi:10.1002/jgrc.20106.

Carrère, L., and F. Lyard (2003), Modeling the barotropic response of the global ocean to atmospheric wind and pressure forcing-comparisons with observations, *Geophys. Res. Lett.*, *30*(6), 1275, doi:10.1029/2002GL016473.

Church, J. A., and N. J. White (2011), Sea-level rise from the late 19th to the early 21st century, *Surv. Geophys.*, *32*(4-5), 585–602.

Dangendorf, S., C. Mudersbach, T. Wahl, and J. Jensen (2013), Characteristics of intra-, inter-annual and decadal sea-level variability and the role of meteorological forcing: The long record of cuxhaven, *Ocean Dyn.*, *63*(2-3), 209–224.

Dangendorf, S., D. Rybski, C. Mudersbach, A. Müller, E. Kaufmann, E. Zorita, and J. Jensen (2014a), Evidence for long-term memory in sea level, *Geophys. Res. Lett.*, *41*, 5564–5571, doi:10.1002/2014GL060538.

Dangendorf, S., F. M. Calafat, A. Arns, T. Wahl, I. D. Haigh, and J. Jensen (2014b), Mean sea level variability in the North Sea: Processes and implications, *J. Geophys. Res. Oceans*, *119*, 6820–6841, doi:10.1002/2014JC009901.

Dangendorf, S., M. Marcos, A. Müller, E. Zorita, R. Riva, K. Berk, and J. Jensen (2015), Detecting anthropogenic footprints in sea level rise, *Nat. Commun.*, *6*, Article number 7849 doi:10.1038/ncomms8849.

Davis, J. L., B. P. Wernicke, and M. E. Tamisiea (2012), On seasonal signals in geodetic time series, *J. Geophys. Res.*, *117*, B01403, doi:10.1029/2011JB008690.

Dee, D., et al. (2011), The era-interim reanalysis: Configuration and performance of the data assimilation system, *Q. J. R. Meteorol. Soc.*, *137*(656), 553–597.

De Jong, P. (1989), Smoothing and interpolation with the state-space model, *J. Am. Stat. Assoc.*, *84*(408), 1085–1088.

Douglas, B. C. (1991), Global sea level rise, *J. Geophys. Res.*, *96*(C4), 6981–6992.

Durbin, J., and S. J. Koopman (2012), *Time Series Analysis by State Space Methods*, 38 pp., Oxford Univ. Press, Oxford, U. K.

Gornitz, V., S. Lebedeff, and J. Hansen (1982), Global sea level trend in the past century, *Science*, *215*(4540), 1611–1614.

Harvey, A. C. (1990), *Forecasting, Structural Time Series Models and the Kalman Filter*, Cambridge Univ. Press, Cambridge, U. K.

Holgate, S. (2007), On the decadal rates of sea level change during the twentieth century, *Geophys. Res. Lett.*, *34*, L01602, doi:10.1029/2006GL028492.

Holgate, S. J., A. Matthews, P. L. Woodworth, L. J. Rickards, M. E. Tamisiea, E. Bradshaw, P. R. Foden, K. M. Gordon, S. Jevrejeva, and J. Pugh (2012), New data systems and products at the permanent service for mean sea level, *J. Coastal Res.*, *29*(3), 493–504.

Hurrell, J. W., Y. Kushnir, G. Ottersen, and M. Visbeck (2003), An overview of the North Atlantic oscillation, in *The North Atlantic Oscillation: Climatic Significance and Environmental Impact, Geophys. Monogr. 134*, edited by J. W. Hurrell et al., pp. 1–36, AGU, Washington, D. C.

Ishii, M., and M. Kimoto (2009), Reevaluation of historical ocean heat content variations with time-varying XBT and MBT depth bias corrections, *J. Oceanogr.*, *65*(3), 287–299.

Jordà, G. (2014), Detection time for global and regional sea level trends and accelerations, *J. Geophys. Res. Oceans*, *119*, 7164–7174, doi:10.1002/2014JC010005.

Koopman, S. J. (1993), Disturbance smoother for state space models, *Biometrika*, *80*(1), 117–126.

Laine, M., N. Latva-Pukkila, and E. Kyrölä (2014), Analysing time-varying trends in stratospheric ozone time series using the state space approach, *Atmos. Chem. Phys.*, *14*(18), 9707–9725.

Landerer, F. W., J. H. Jungclaus, and J. Marotzke (2007), Regional dynamic and steric sea level change in response to the ipcc-a1b scenario, *J. Phys. Oceanogr.*, *37*(2), 296–312.

Mantua, N. J., S. R. Hare, Y. Zhang, J. M. Wallace, and R. C. Francis (1997), A pacific interdecadal climate oscillation with impacts on salmon production, *Bull. Am. Meteorol. Soc.*, *78*(6), 1069–1079.

Nerem, R., and G. Mitchum (2002), Estimates of vertical crustal motion derived from differences of TOPEX/POSEIDON and tide gauge sea level measurements, *Geophys. Res. Lett.*, *29*(19), 1934, doi:10.1029/2002GL015037.

Plag, H.-P., and M. Tsimplis (1999), Temporal variability of the seasonal sea-level cycle in the North Sea and Baltic Sea in relation to climate variability, *Global Planet. Change*, *20*(2), 173–203.

Proudman, J. (1960), The condition that a long-period tide shall follow the equilibrium-law, *Geophys. J. Int.*, *3*(2), 244–249.

Pugh, D., and P. Woodworth (2014), *Sea-Level Science: Understanding Tides, Surges, Tsunamis and Mean Sea-Level Changes*, Cambridge Univ. Press, Cambridge, U. K.

Schweppe, F. C. (1965), Evaluation of likelihood functions for Gaussian signals, *IEEE Trans. Inf. Theory*, *11*(1), 61–70.

Shumway, R. H., and D. S. Stoffer (1982), An approach to time series smoothing and forecasting using the EM algorithm, *J. Time Series Anal.*, *3*(4), 253–264.

Wahl, T., J. Jensen, T. Frank, and I. D. Haigh (2011), Improved estimates of mean sea level changes in the German bight over the last 166 years, *Ocean Dyn.*, *61*(5), 701–715.

Wahl, T., I. Haigh, P. Woodworth, F. Albrecht, D. Dillingh, J. Jensen, R. Nicholls, R. Weisse, and G. Wöppelmann (2013), Observed mean sea level changes around the North Sea coastline from 1800 to present, *Earth Sci. Rev.*, *124*, 51–67.

Watson, M. W., and R. F. Engle (1983), Alternative algorithms for the estimation of dynamic factor, mimic and varying coefficient regression models, *J. Econometrics*, *23*(3), 385–400.

Wenzel, M., and J. Schröter (2014), Global and regional sea level change during the 20th century, *J. Geophys. Res. Oceans*, *119*, 7493–7508, doi:10.1002/2014JC009900.

Wolter, K., and M. S. Timlin (1993), Monitoring ENSO in COADS with a seasonally adjusted principal component index, in *Proceedings of the 17th Climate Diagnostics Workshop*, pp. 52–57, NOAA/NMC/CAC, NSSL, Oklahoma Clim. Surv., CIMMS and the School of Meteor., Univ. of Oklahoma, Norman, Okla. [Available at: http://www.esrl.noaa.gov/psd/enso/mei/WT1.pdf.]

Woodworth, P., N. J. White, S. Jevrejeva, S. Holgate, J. Church, and W. Gehrels (2009), Evidence for the accelerations of sea level on multi-decade and century timescales, *Int. J. Climatol.*, *29*(6), 777–789.

Woodworth, P. L. (2011), A note on the nodal tide in sea level records, *J. Coastal Res.*, *28*(2), 316–323.

Wunsch, C., and D. Stammer (1997), Atmospheric loading and the oceanic'' inverted barometer'' effect, *Rev. Geophys.*, *35*(1), 79–107.

Zijl, F., M. Verlaan, and H. Gerritsen (2013), Improved water-level forecasting for the northwest European shelf and North Sea through direct modelling of tide, surge and non-linear interaction, *Ocean Dyn.*, *63*(7), 823–847.